Nonadiabatic tunneling via conical intersections and the role of the geometric phase

Changjian Xie, David R. Yarkony, and Hua Guo

Phys. Rev. A **95**, 022104 — Published 6 February 2017

DOI: 10.1103/PhysRevA.95.022104

Nonadiabatic Tunneling *via* Conical Intersections and the Role of the Geometric Phase

Changjian Xie,[†] David R. Yarkony,[#] and Hua Guo*[,†,%]

[†]*Department of Chemistry and Chemical Biology, University of New Mexico, Albuquerque, New Mexico 87131*

[#]*Department of Chemistry, Johns Hopkins University, Baltimore, Maryland 21218*

[%]*Department of Physics and Astronomy, University of New Mexico, Albuquerque, New Mexico 87131*

Abstract

As a ubiquitous quantum effect, tunneling has attracted attention ever since the dawn of quantum mechanics. However, recent evidence suggests that nonadiabatic atomic tunneling near a conical intersection (CI) behaves differently from its adiabatic counterpart, producing lifetime differences up to two orders of magnitude. Using two-dimensional models, we demonstrate here that the failure of the adiabatic model in describing tunneling near a CI can be attributed largely to the neglect of the geometric phase, which is associated with the adiabatic electronic wavefunction transported around a CI. The geometric phase-induced destructive interference among wavefunctions following different paths around the CI, manifested as a node in the adiabatic wavefunction, retards tunneling.

I. Introduction

Tunneling describes wave-like behavior of a quantum particle in penetrating classically forbidden regions. This quantum effect is omnipresent in physics, chemistry, and biology.[1] In molecular physics, tunneling of a light atom is conventionally characterized by the nuclear Schrödinger equation on an adiabatic potential energy surface (PES), namely the dependence of electronic energy on nuclear coordinates. This separation of electronic and nuclear motions, originally introduced by Born and Oppenheimer (BO),[2] is justified by the large mass disparity and has since become the standard paradigm in discussing molecular spectroscopy and reaction dynamics.

However, this adiabatic picture becomes inadequate near electronic degeneracy, such as a conical intersection (CI).[3-6] Near a CI, electronic states interact strongly *via* nonadiabatic couplings (NACs), which are ignored in the BO approximation. Furthermore, a real-valued adiabatic electronic wavefunction changes sign when transported around a CI, an effect termed the geometric (or Berry's) phase (GP), which renders the electronic wavefunction double-valued.[7-11] Since the total wavefunction must be single-valued, this double-valuedness in the electronic wavefunction requires the nuclear wavefunction to be double-valued as well. Since the GP is associated with nuclear motion, it has important consequences in spectroscopy and dynamics for systems affected by CIs.[7, 8, 12-33] Interestingly, GP is implicitly included in the diabatic representation, which is related to the adiabatic representation through a unitary transformation that minimizes the NACs.[34-36]

We focus here on a seldom considered situation, in which metastable vibronic states prepared by photoexcitation decay *via* tunneling near a CI. This scenario is common in

photochemistry,[5] because the electronically excited states involved are more likely to exhibit CIs than their ground state counterparts. It is tempting to model such dynamics using a single adiabatic PES if the CI has a much higher energy, because the upper adiabat is energetically "inaccessible", and indeed such models have been in wide use.[37-39] However, recent studies suggest that nonadiabatic tunneling behaves very differently from adiabatic tunneling. In one study,[28, 29] it was shown that in a double-well Jahn-Teller system formed by a CI, the spatial delocalization of a wave packet seen in the adiabatic model is severely curtailed by the inclusion of GP. In another investigation from our groups,[40] it was demonstrated that nonadiabatic tunneling decay of the lowest vibronic level of phenol (C_6H_5OH) in the S_1 state, which forms a CI with the S_2 state near the Franck-Condon region,[41-46] proceeds much more slowly than that predicted by the adiabatic model. While the lifetime with the GP is in reasonably good agreement with experiment, the one without the GP is about two orders of magnitude faster.[40] These surprising results called into question the appropriateness of many existing adiabatic models for treating tunneling in photochemical systems.[37-39] Here, we demonstrate that the overestimate of the tunneling rate in phenol photodissociation by the adiabatic model is largely due to the neglect of the GP, and that with the inclusion of the GP much of the error is recovered. We follow with a discussion of the mechanistic aspects of nonadiabatic tunneling.

II. Theory

We adapt here a two-dimensional (2D) model, in which the CI between two interacting electronic states is simply a point. This model represents a special case, where adiabatic NAC is completely removable by the adiabatic-to-diabatic (AtD) transformation.[6] The diabatic Hamiltonian assumes the following form ($\hbar = 1$):

$$\hat{H}^{(d)} = \begin{pmatrix} \hat{T} & 0 \\ 0 & \hat{T} \end{pmatrix} + \begin{pmatrix} V_{11} & V_{12} \\ V_{12} & V_{22} \end{pmatrix}, \tag{1}$$

where $\hat{T} = -\nabla^2 / 2 = -(\partial^2 / \partial x^2 + \partial^2 / \partial y^2) / 2$ is the kinetic energy operator (KEO) while the potential energy operator (PEO) is a 2×2 matrix. The corresponding adiabatic Hamiltonian

$$\hat{H}^{(a)} = \begin{pmatrix} \hat{T} + \hat{\tau}_{11} & i\hat{\tau}_{12} \\ -i\hat{\tau}_{21} & \hat{T} + \hat{\tau}_{22} \end{pmatrix} + \begin{pmatrix} W_{-} & 0 \\ 0 & W_{+} \end{pmatrix} \tag{2}$$

is obtained *via* the following unitary AtD transformation

$$U = \begin{pmatrix} \cos\theta & \sin\theta \\ -\sin\theta & \cos\theta \end{pmatrix}, \tag{3}$$

where θ is the mixing angle between two diabatic states:

$$\theta = \frac{1}{2}\arctan\frac{2V_{12}}{V_{11} - V_{22}}. \tag{4}$$

In the adiabatic representation, the PEO is diagonal

$$W_{\pm} = \frac{1}{2}(V_{11} + V_{22}) \pm \frac{1}{2}\sqrt{(V_{11} - V_{22})^2 + 4V_{12}^2}, \tag{5}$$

and the NAC includes the scalar diagonal BO correction (DBOC)

$$\hat{\tau}_{11} = \hat{\tau}_{22} = \frac{1}{2}\nabla\theta \cdot \nabla\theta, \tag{6}$$

and vectorial derivative coupling (DC)

$$\hat{\tau}_{12} = \hat{\tau}_{21} = \frac{1}{2}\left((-i\nabla)^{\dagger} \cdot \nabla\theta + \nabla\theta \cdot (-i\nabla) \right), \tag{7}$$

where † denotes Hermitian conjugation.

Numerically, the adiabatic model is difficult to handle because at the CI the NAC diverges and the PESs ($W_{\pm}$) are not differentiable. Consequently, most nonadiabatic calculations are performed in the diabatic representation.[3, 47] Since we are interested in quantifying the effect of GP, we focus on Eq. (2), but recognize that the diabatic representation in Eq. (1) provides the exact solution to which all approximate adiabatic models can be compared. Although related by a unitary transformation, the Hamiltonians in Eqs. (1) and (2) have different, single-valued *vs*. double-valued, boundary conditions.[29] To enforce the double-valued boundary condition of the adiabatic wavefunction, we follow Mead and Truhlar[9] and introduce a position-dependent phase factor $e^{in\theta(x,y)}$ (n is an integer) into the adiabatic wave function, which makes the total wave function single-valued and leads to the following Hamiltonian with a vector or gauge potential

$$\hat{H}^{(a)}_{GP} = e^{-in\theta}\hat{H}^{(a)}e^{in\theta} = \begin{pmatrix} \hat{T} + \hat{\tau}^{\mathrm{GP}}_{11} & i\hat{\tau}^{\mathrm{GP}}_{12} \\ -i\hat{\tau}^{\mathrm{GP}}_{21} & \hat{T} + \hat{\tau}^{\mathrm{GP}}_{22} \end{pmatrix} + \begin{pmatrix} W_{-} & 0 \\ 0 & W_{+} \end{pmatrix}, \tag{8}$$

where

$$\hat{\tau}^{\mathrm{GP}}_{11} = \hat{\tau}^{\mathrm{GP}}_{22} = \hat{\tau}_{11} + \left(e^{-in\theta}\hat{T}e^{in\theta} - \hat{T} \right), \tag{9}$$

$$\hat{\tau}^{\mathrm{GP}}_{12} = \hat{\tau}^{\mathrm{GP}}_{21} = e^{-in\theta}\hat{\tau}_{12}e^{in\theta}. \tag{10}$$

This two-state adiabatic model with a vector potential is denoted as Model IA for odd n values, and IB for even n values.[9]

We further examine a single-state adiabatic model (Model II), in which n=1 and the upper adiabat and associated off-diagonal terms in Eq. (8) are removed:

$$\hat{H}^{(a)}_{GP-} = \hat{T} + \hat{\tau}^{\mathrm{GP}}_{11} + W_{-} = \hat{T} + \nabla\theta\cdot\nabla\theta + \frac{1}{2}\left(\left(-i\nabla\right)^{\dagger}\cdot\nabla\theta + \nabla\theta\cdot\left(-i\nabla\right)\right) + W_{-}. \tag{11}$$

In Model IIA or IIB, the DBOC term is either retained or removed. Finally, Model IIIA is defined by the Hamiltonian in Eq. (11) without the GP term:

$$\hat{H}^{(a)}_{-} = \hat{T} + \hat{\tau}_{11} + W_{-} = \hat{T} + \frac{1}{2}\nabla\theta\cdot\nabla\theta + W_{-}, \tag{12}$$

and Model IIIB further ignores the DBOC.

All calculations are carried out in polar coordinates (ρ, φ), $x = \rho\cos\varphi$ and $y = \rho\sin\varphi$, with the CI at the origin. This choice allows a dense grid near the singularity (ρ=0) of the adiabatic Hamiltonians. The KEO assumes the following form:

$$\hat{T} = -\frac{1}{2}\left(\frac{\partial^2}{\partial\rho^2} + \frac{1}{4\rho^2} + \frac{1}{\rho^2}\frac{\partial^2}{\partial\varphi^2}\right), \tag{13}$$

and the wavefunction is expanded in a direct-product basis:

$$\psi(\rho,\varphi) = \frac{1}{\sqrt{2\pi\rho}}\sum_{m,n} C_{mn} R_n(\rho) e^{im\varphi} = \sum_{m,n} C'_{mn}\left|nm\right\rangle, m = 0,\pm1,\pm2,... \tag{14}$$

with the orthonormality

$$\int_0^{\infty} R_n(\rho) R_{n'}(\rho) d\rho = \delta_{nn'}. \tag{15}$$

The radial basis function $R_n(\rho)$ is chosen as[48]

$$R_n(\rho)=\sqrt{\frac{2}{b-a}}\sin[\frac{n\pi(\rho-a)}{b-a}],\qquad n=1,2,... \tag{16}$$

where a and b are the minimum and maximum of the ρ range, respectively. So the KEO matrix elements represented in the basis of Eq. (14) are

$$\begin{aligned}
&[T]_{nm,n'm'}=\langle nm|\hat{T}|n'm'\rangle \\
&=-\frac{1}{2}\left(\langle nm|\frac{\partial^2}{\partial\rho^2}|n'm'\rangle+\langle nm|\frac{1}{4\rho^2}|n'm'\rangle+\langle nm|\frac{1}{\rho^2}\frac{\partial^2}{\partial\varphi^2}|n'm'\rangle\right) \\
&=-\frac{1}{2}\left([T_1]_{nm,n'm'}+[T_2]_{nm,n'm'}+[T_3]_{nm,n'm'}\right),
\end{aligned} \tag{17}$$

where

$$[T_1]_{nm,n'm'}=-\left(\frac{n\pi}{b-a}\right)^2\delta_{nn'}\delta_{mm'}, \tag{18a}$$

$$[T_2]_{nm,n'm'}=\delta_{mm'}\frac{1}{4}\int_a^b R_n(\rho)\frac{1}{\rho^2}R_{n'}(\rho)d\rho, \tag{18b}$$

$$[T_3]_{nm,n'm'}=-m^2\delta_{mm'}\int_a^b R_n(\rho)\frac{1}{\rho^2}R_{n'}(\rho)d\rho. \tag{18c}$$

The one-dimensional (1D) integrals in Eq. (18b) and (18c) can be readily calculated by the Gauss-Legendre quadrature. The matrix elements of PEO are computed by 2D Gauss-Legendre quadrature:

$$[V]_{nm,n'm'}=\langle nm|V|n'm'\rangle=\frac{1}{2\pi}\int_0^{2\pi}\int_a^b R_n(\rho)V(\rho,\varphi)R_{n'}(\rho)e^{i(m'-m)\varphi}d\rho d\varphi. \tag{19}$$

The matrix elements of the DBOC terms in polar coordinates are

$$
\begin{aligned}
[\tau_{11}]_{nm,n'm'} = [\tau_{22}]_{nm,n'm'} &= \frac{1}{4\pi}\int_0^{2\pi}\int_a^b R_n(\rho)\frac{\partial\theta}{\partial\rho}\cdot\frac{\partial\theta}{\partial\rho}R_{n'}(\rho)e^{i(m'-m)\varphi}d\rho d\varphi \\
&+\frac{1}{4\pi}\int_0^{2\pi}\int_a^b R_n(\rho)\frac{1}{\rho^2}\frac{\partial\theta}{\partial\varphi}\cdot\frac{\partial\theta}{\partial\varphi}R_{n'}(\rho)e^{i(m'-m)\varphi}d\rho d\varphi
\end{aligned}
\tag{20}
$$

and the DC terms are

$$
\begin{aligned}
[\tau_{12}]_{nm,n'm'} &= [\tau_{21}]_{nm,n'm'} \\
&= \frac{i}{4\pi}\int_0^{2\pi}\int_a^b \frac{dR_n(\rho)}{d\rho}\frac{\partial\theta}{\partial\rho}R_{n'}(\rho)e^{i(m'-m)\varphi}d\rho d\varphi \\
&-\frac{i}{4\pi}\int_0^{2\pi}\int_a^b R_n(\rho)\frac{\partial\theta}{\partial\rho}\frac{dR_{n'}(\rho)}{d\rho}e^{i(m'-m)\varphi}d\rho d\varphi \\
&+\frac{(m+m')}{4\pi}\int_0^{2\pi}\int_a^b R_n(\rho)\frac{1}{\rho^2}\frac{\partial\theta}{\partial\varphi}R_{n'}(\rho)e^{i(m'-m)\varphi}d\rho d\varphi.
\end{aligned}
\tag{21}
$$

The matrix elements in Eqs. (20) and (21) are both computed using the 2D Gauss-Legendre quadrature. Matrix elements of other related operators can be obtained in an analogous way.

We first examine the well-studied 2D Jahn-Teller model:[3, 7, 28]

$$V_{11} = \frac{\omega_1^2}{2}\left(x+\frac{a}{2}\right)^2 + \frac{\omega_2^2}{2}y^2, \tag{22a}$$

$$V_{22} = \frac{\omega_1^2}{2}\left(x-\frac{a}{2}\right)^2 + \frac{\omega_2^2}{2}y^2 - \Delta, \tag{22b}$$

$$V_{12} = cy\,. \tag{22c}$$

The PESs are displayed in Figure 1(a) for a typical set of parameters. The unique topological feature is a CI located at the symmetry plane in the coupling mode (y=0) flanked by two equivalent and energetically lower saddle points (y > and < 0), which form a significant adiabatic

barrier along the tuning mode (x) between the two wells. The eigen-problem was solved by direct diagonalization of the Hamiltonian matrix.

To investigate dissociative tunneling dynamics, such as in phenol photodissociation,[40] we replace V_{22} in Eqs. (22b) with a repulsive form and introduce a Gaussian shaped V_{12}:

$$V_{22} = Ae^{-\alpha(x+b)} + \frac{\omega_2^2}{2} y^2 - \Delta, \tag{23a}$$

$$V_{12} = cy \cdot \exp[-(x - x_{\mathrm{CI}})^2 / 2\sigma_x^2] \cdot \exp[-y^2 / 2\sigma_y^2]. \tag{23b}$$

The corresponding PESs are displayed in Figure 1(b), which also has the CI flanked by two lower but equi-energetic saddle points. The low-lying vibrational levels in the left well can only tunnel as they below both the CI (2.603 a.u.) and saddle points (1.878 a.u.).

For this dissociative problem, the wave packet is propagated using the Chebyshev propagator[49]

$$\psi_k = 2DH_s\psi_{k-1} - D^2\psi_{k-2}, \quad k \geq 2, \tag{24}$$

with $\psi_1 = DH_s\psi_0$ and $\psi_0 = \psi_i$, where ψ_i is the eigenfunction of the diabatic Hamiltonian $\hat{T} + V_{11}$. The Hamiltonian matrix is scaled to the spectral range of (-1,1) via $H_s = (H - \bar{H})/\Delta H$, in which the spectral medium ($\bar{H} = (H_{\max} + H_{\min})/2$) and half width ($\Delta H = (H_{\max} - H_{\min})/2$) were determined by the spectral extrema, $H_{\max}$ and $H_{\min}$.[50] Here, the former was determined by convergence. D is the damping function, which is used to avoid reflection at the edge of the radial grids. To extract tunneling lifetimes, a low-storage filter diagonalization method[49] was used to determine the complex energies (E-$i\Gamma/2$) of the lowest-lying state. To this end, the

Chebyshev correlation functions are used to build an energy-localized Hamiltonian matrix, from which the complex energies of the resonances are obtained by diagonalization.[49]

III. Results and discussion

For the Jahn-Teller model, 35 and 31 functional bases were used for the ρ and φ coordinates, respectively. 1000 and 1000 Gauss-Legendre quadrature points were used in ranges [0.0, 8.0] a.u. and [0.0, 2π] for the two degrees of freedom. The large grids used in the integration are due to the difficulties associated with converging the matrix elements of divergent operators. The derivatives of θ were obtained numerically by the central-difference algorithm.

Table I compares low-lying eigenvalues of the exact two-state diabatic model with those of the adiabatic models. These levels lie much lower than the CI (4.495 a.u). Model IA yields identical results as the diabatic model, as they must, thus validating our algorithm. These results also indicate that this model is gauge invariant as all odd (even) n values give the same results, corresponding to the inclusion (exclusion) of the GP. When DBOC is included, the values from Model IIA are quite accurate, but those from Model IIIA have larger errors. Ignoring DBOC leads to additional errors in Models IIB and IIIB.

To illustrate the role played by GP, adiabatic wavefunctions of the lowest-lying state obtained from various models are compared in Figure 2. The most striking feature in both the two-state diabatic (Figure 2(a)) and one-state GP-corrected adiabatic (Figure 2(b)) models is the node on the left side of the CI (x<0), which is a hallmark of GP.[15, 16, 27-29, 31] In the diabatic representation, the transition between V_{11} and V_{22} necessitates a change of symmetry in the wavefunction as the coupling term (V_{12}) is antisymmetric with respect to y=0. In the adiabatic representation without GP (Eq. (12)), on the other hand, such symmetry change is absent, as

evidenced by the nodeless structure of the adiabatic wavefunction (Figure 2(c)). The node is recovered when GP is included in the adiabatic model (Eq. (11)). These conclusions are consistent with the recent work of Izmaylov and coworkers,[28, 29] who examined the time-dependent behavior of similar models. These model studies clearly suggest that the neglect of the GP in the adiabatic representation leads to qualitatively incorrect results.

In our calculations of the dissociative system, the parameters (in a.u.) of model PESs are ω_1=1, ω_2=1, a=4, A=5.0, b=-11, Δ=12, α=0.1, c=2, σ_x=1.274, and σ_y=0.849. 45 and 75 bases were used for the ρ and φ coordinates, respectively. 1000 and 2000 Gauss-Legendre quadrature points were used in ranges [0.0, 15.0] a.u. and [0.0, 2π] for the ρ and φ coordinates, respectively. A damping function $D=\exp[-0.0027(x-9.0)^2]$ for x>9.0 a.u. was used to avoid reflection.

In Figure 3, lifetimes obtained from both diabatic and adiabatic models are compared, again using the former as a benchmark. The Model IIIB yields lifetimes approximately two orders of magnitude too short, similar to our previous observation for phenol photodissociation.[40] The lifetimes with only the DBOC included (Model IIIA) are better than the standard adiabatic ones without GP and DBOC. The inclusion of the GP (Model IIB) significantly improves the results, suggesting that it captures the essential physics, similar to the bound system discussed above. The lifetimes from the single-state adiabatic model with both GP and DBOC (Model IIA) agree best with the exact results. The remaining errors are necessarily due to the neglect of the upper adiabat, as suggested by the bound system results.

As expected, the poor performance of the adiabatic models without the GP stems from the symmetry change introduced by the vector potential. To this end, wavefunctions from the two adiabatic models are compared in Figure 4. Without the GP, the wavefunction is nodeless

throughout (Figure 4(b)), as the tunneling follows the adiabatic pathway under the barrier. However, the inclusion of the GP leads to the development of a node at y=0 (x>0) (Figure 4(a)), as noted in previous studies of similar problems.[15, 27, 31, 40, 42]

To shed further light on the nodal structure in the GP-corrected adiabatic wavefunction, we adapt the topological approach of Althorpe and coworkers[51, 52] to unwind the dissociation wavefunction. The essential idea of this approach is to separate the wavefunction into two components with even and odd loops around the CI: Φ_e and Φ_o. These two wavefunctions correspond to clockwise and counter-clockwise Feynman paths around the CI.[31] Numerically, these two wavefunctions can be obtained from the adiabatic wavefunctions on the lower adiabat obtained with and without the GP: Φ_{GP} and Φ_{NGP}:

$$\Phi_e = \frac{1}{\sqrt{2}}\left(\Phi_{GP} + \Phi_{NGP}\right), \tag{25a}$$

$$\Phi_o = \frac{1}{\sqrt{2}}\left(\Phi_{NGP} - \Phi_{GP}\right). \tag{25b}$$

The former (Φ_{GP}) can be obtained in this 2D model from the diabatic Hamiltonian in which the GP is implicitly included, while the latter (Φ_{NGP}) from the corresponding adiabatic Hamiltonian without GP. The phase difference of the two wavefunctions is determined by

$$\cos\left(\phi_e - \phi_o\right) = \frac{\left|\Phi_e\right|^2 + \left|\Phi_o\right|^2 - 2\left|\Phi_{GP}\right|^2}{2\left|\Phi_e\right|\left|\Phi_o\right|}. \tag{26}$$

By symmetry of the system, the clockwise and counter-clockwise wavefunctions of the adiabatic system have the same amplitude and phase at y=0, in which the interference is constructive. The

addition of the GP changes the relative phase of Φ_e and Φ_o, and converts the constructive interference to a destructive one, which leads to the node in the GP-corrected adiabatic wavefunction. From Figure 4(c), it is clear that the wavefunctions Φ_e and Φ_o are in phase for y=0 for x>0, so that Φ_{GP} has a node. The destructive interference between Φ_e and Φ_o retards tunneling, thus providing a definitive mechanism for the large difference between nonadiabatic and adiabatic lifetimes observed in our recent work.[40] We further note that destructive inference is also responsible for the experimentally observed propensity of odd quantum numbers for out-of-plane vibrations in the phenoxyl product.[26, 31] All wave packets in the above discussion were represented in the time domain. The time-dependent wave packet can be obtained by assembling the Chebyshev wave packets (ψ_k) using the method of Tal-Ezer and Kosloff.[50]

To further understand the mechanism of nonadiabatic tunneling, the parameter σ_x of V_{12} is varied in such a way that its impact on the adiabatic barrier is minimal. In Figure 3, it is seen that nonadiabatic tunneling is largely controlled by the width of the nonadiabatic coupling, in sharp contrast to adiabatic tunneling, which is largely determined by the height and width of the barrier. The dependence of the tunneling lifetime on nonadiabatic coupling can be readily understood as the diabatic coupling (V_{12}) enables a transient population on the high-energy V_{22} state in the Franck-Condon region, which is subjected to a repulsive force towards the dissociation asymptote. This nonadiabatic mechanism also explains the isotope effect observed in our recent work,[40] due to its more compact wavefunction in deuterated phenol, which is more difficult to access V_{12} as it is farther from the CI. In the GP-corrected adiabatic models, these effects are largely recovered through the DBOC and GP terms.

IV. Summary

Despite the conventional wisdom that low-energy dynamics can be effectively described by the Born-Oppenheimer approach, it is shown here and elsewhere that tunneling at energies much below the CI is still significantly affected by the GP. In this work, 2D models have been used to elucidate the role of the GP in affecting tunneling dynamics near a CI. The GP is introduced in adiabatic models by a coordinate-dependent phase factor. It is convincingly shown that the neglect of the GP in the adiabatic model, as done in several recent models, gives rise to a qualitatively incorrect characterization of nonadiabatic tunneling in both bound and dissociative systems. The inclusion of the GP in an adiabatic model enables destructive interference, as evidenced by the nodal structure in the wavefunction. The destructive interference retards the tunneling facilitated dissociation. However, it is also worth pointing out that the neglect of the upper adiabat introduces sufficient errors that a single-state adiabatic treatment cannot reach a quantitative agreement with the results obtained from a two-state diabatic calculation. The results presented here motivate us to rethink how nonadiabatic tunneling should be treated in the adiabatic representation. The correct and efficient characterization of the GP in non-adiabatic dynamics could help us to better understand a wide array of issues in molecular physics, and to explore new ways to control the dynamics.

While the 2D models shed valuable light on the GP effects in spectroscopy and dynamics in systems affected by CIs, the methodology used here needs be significantly modified to treat real systems that have higher dimensionalities. Because the seam of a CI spans N-2 dimensions, it is difficult to find a high-dimensional path encircling the CI, which is needed for defining the vector potential. In many real systems studied so far (*e.g.* X_3), the vector potential has been defined in hyperspherical coordinates as a function of a hyper-angle by taking advantage of the

intrinsic high symmetry in such systems.[9, 13, 19] For molecules without high symmetry, it is not clear how this hyper-angle can be defined. To solve this problem, we have recently proposed a new approach in which the vector potential can be uniquely defined by the derivative of the line integral in a removable approximation to the *ab initio* DC,[53] which can be accurately determined by fitting *ab initio* data.[54] It has been demonstrated that this two-state description of the nonadiabatic system is possible, despite the well-known fact that the *ab initio* derivative coupling is nonremovable and consequently has a curl so that its line integral is path dependent.[35, 36, 55] However, even with a clear definition of the vector potential, the treatment of the singularities at the seam of the CI in the adiabatic Hamiltonian, with and without the GP, remain extremely challenging. Efficient numerical algorithms are needed to solve the corresponding multi-dimensional adiabatic dynamics.

Acknowledgments: We thank Stuart Althorpe, Foudhil Bouakline, Artur Izmaylov, and Brian Kendrick for stimulating discussions and DOE (DE-SC0015997) for financial support.

References:

1. T. Miyazaki, *Atom Tunneling Phenomena in Physics, Chemistry and Biology*. (Springer, Berlin, 2004).
2. M. Born and R. Oppenheimer, Ann. Phys. **84**, 0457 (1927).
3. H. Köppel, W. Domcke and L. S. Cederbaum, Adv. Chem. Phys. **57**, 59 (1984).
4. D. R. Yarkony, Rev. Mod. Phys. **68**, 985 (1996).
5. W. Domcke, D. R. Yarkony and H. Köppel, *Conical Intersections: Electronic Structure, Dynamics and Spectroscopy*. (World Scientific, Singapore, 2004).
6. M. Baer, *Beyond Born-Oppenheimer: Electronic Nonadiabatic Coupling Terms and Conical Intersections*. (Wiley, New Jersey, 2006).
7. H. C. Longuet-Higgins, U. Öpik, M. H. L. Pryce and R. A. Sack, Proc. Royal Soc. A (London) **244**, 1 (1958).
8. G. Herzberg and H. C. Longuet-Higgins, Discuss. Faraday Soc. **35**, 77 (1963).
9. C. A. Mead and D. G. Truhlar, J. Chem. Phys. **70**, 2284 (1979).
10. M. V. Berry, Proc. Royal Soc. A (London) **392**, 45 (1984).
11. F. S. Ham, Phys. Rev. Lett. **58**, 725 (1987).
12. C. A. Mead, J. Chem. Phys. **72**, 3839 (1980).
13. B. Lepetit and A. Kuppermann, Chem. Phys. Lett. **166**, 581 (1990).
14. H. Koizumi and S. Sugano, J. Chem. Phys. **101**, 4903 (1994).
15. J. Schön and H. Köppel, J. Chem. Phys. **103**, 9292 (1995).
16. V. J. Barclay, C. E. Dateo, I. P. Hamilton, B. Kendrick, R. T Pack and D. W. Schwenke, J. Chem. Phys. **103**, 3864 (1995).
17. R. Baer, D. M. Charutz, R. Kosloff and M. Baer, J. Chem. Phys. **105**, 9141 (1996).
18. B. Kendrick and R. T. Pack, J. Chem. Phys. **104**, 7475 (1996).
19. B. Kendrick, Phys. Rev. Lett. **79**, 2431 (1997).
20. A. J. C. Varandas and H. G. Yu, J. Chem. Soc., Faraday Trans. **93**, 819 (1997).
21. B. K. Kendrick, J. Chem. Phys. **112**, 5679 (2000).
22. Z. Xu, M. Baer and A. J. C. Varandas, J. Chem. Phys. **112**, 2746 (2000).
23. D. Babikov, B. K. Kendrick, P. Zhang and K. Morokuma, J. Chem. Phys. **122**, 044315 (2005).
24. J. C. Juanes-Marcos and S. C. Althorpe, J. Chem. Phys. **122**, 204324 (2005).
25. F. Bouakline, S. C. Althorpe and D. Peláez Ruiz, J. Chem. Phys. **128**, 124322 (2008).
26. M. G. D. Nix, A. L. Devine, R. N. Dixon and M. N. R. Ashfold, Chem. Phys. Lett. **463**, 305 (2008).
27. R. N. Dixon, T. A. A. Oliver and M. N. R. Ashfold, J. Chem. Phys. **134**, 194303 (2011).
28. I. G. Ryabinkin and A. F. Izmaylov, Phys. Rev. Lett. **111**, 220406 (2013).
29. L. Joubert-Doriol, I. G. Ryabinkin and A. F. Izmaylov, J. Chem. Phys. **139**, 234103 (2013).
30. I. G. Ryabinkin, L. Joubert-Doriol and A. F. Izmaylov, J. Chem. Phys. **140**, 214116 (2014).
31. F. Bouakline, Chem. Phys. **442**, 31 (2014).
32. B. K. Kendrick, J. Hazra and N. Balakrishnan, Nat. Commun. **6**, 7918 (2015).
33. B. K. Kendrick, J. Hazra and N. Balakrishnan, Phys. Rev. Lett. **115**, 153201 (2015).
34. F. T. Smith, Phys. Rev. **179**, 111 (1969).
35. C. A. Mead and D. G. Truhlar, J. Chem. Phys. **77**, 6090 (1982).
36. M. Baer, Chem. Phys. **259**, 123 (2000).
37. G. A. Pino, A. N. Oldani, E. Marceca, M. Fujii, S. I. Ishiuchi, M. Miyazaki, M. Broquier, C. Dedonder and C. Jouvet, J. Chem. Phys. **133**, 124313 (2010).
38. T. N. V. Karsili, A. M. Wenge, S. J. Harris, D. Murdock, J. N. Harvey, R. N. Dixon and M. N. R. Ashfold, Chem. Sci. **4**, 2434 (2013).
39. X. Xu, J. J. Zheng, K. R. Yang and D. G. Truhlar, J. Am. Chem. Soc. **136**, 16378 (2014).

40. C. Xie, J. Ma, X. Zhu, D. R. Yarkony, D. Xie and H. Guo, J. Am. Chem. Soc. **138**, 7828 (2016).
41. A. L. Sobolewski and W. Domcke, J. Phys. Chem. A **105**, 9275 (2001).
42. Z. Lan, W. Domcke, V. Vallet, A. L. Sobolewski and S. Mahapatra, J. Chem. Phys. **122**, 224315 (2005).
43. M. N. R. Ashfold, B. Cronin, A. L. Devine, R. N. Dixon and M. G. D. Nix, Science **312**, 1637 (2006).
44. K. R. Yang, X. Xu, J. J. Zheng and D. G. Truhlar, Chem. Sci. **5**, 4661 (2014).
45. X. Zhu and D. R. Yarkony, J. Chem. Phys. **144**, 024105 (2016).
46. X. Zhu, C. L. Malbon and D. R. Yarkony, J. Chem. Phys. **144**, 124312 (2016).
47. H. Guo and D. R. Yarkony, Phys. Chem. Chem. Phys. **18**, 26335 (2016).
48. D. T. Colbert and W. H. Miller, J. Chem. Phys. **96**, 1982 (1992).
49. H. Guo, Rev. Comput. Chem. **25**, 285 (2007).
50. H. Tal-Ezer and R. Kosloff, J. Chem. Phys. **81**, 3967 (1984).
51. J. C. Juanes-Marcos, S. C. Althorpe and E. Wrede, Science **309**, 1227 (2005).
52. S. C. Althorpe, J. Chem. Phys. **124**, 084105 (2006).
53. C. L. Malbon, X. Zhu, H. Guo and D. R. Yarkony, J. Chem. Phys. **145**, 234111 (2016).
54. M. Baer, J. Chem. Phys. **107**, 2694 (1997).
55. D. R. Yarkony, J. Chem. Phys. **105**, 10456 (1996).

Table I. Low-lying eigenvalues (in a.u.) for diabatic and adiabatic models. The parameters (in a.u.) used in model PESs: ω_1=1, ω_2=1, a=6, Δ=0.01, c=3.

Two-State Diabatic (Exact)	Two-State Adiabatic (Model I)		One-State Adiabatic with GP (Model II)		One-State Adiabatic without GP (Model III)	
	odd n (IA)	even n (IB)	with DBOC (IIA)	without DBOC (IIB)	with DBOC (IIIA)	without DBOC (IIIB)
0.50960	0.50960	0.49501	0.50985	0.49265	0.49501	0.47738
0.51462	0.51462	0.56173	0.51487	0.49765	0.56233	0.54592
0.64067	0.64067	0.56192	0.64163	0.62612	0.56252	0.54610
0.64067	0.64067	0.74515	0.64163	0.62612	0.74647	0.73185
0.87189	0.87189	0.74515	0.87353	0.85977	0.74647	0.73185
0.87189	0.87189	1.01800	0.87353	0.85977	1.01993	1.00696

Figure Captions (all single-column figures):

Figure 1. Adiabatic PESs ($W_{\pm}$) for two typical sets of parameters (a.u.): (a) ω_1=1, ω_2=1, a=6, Δ=0, and c=1; (b) ω_1=1, ω_2=1, a=4, A=5.0, b=-11, Δ=12.0, α=0.1; c=2, σ_x=1.699 and σ_y= 0.849.

Figure 2. Modulus of the adiabatic wavefunctions (|Φ|) of the lowest-lying state in the diabatic model (a), one-state adiabatic model with GP (Model IIA) (b), and one-state adiabatic model without GP (Model IIIA) (c).

Figure 3. Lifetimes (ps) of the lowest-lying state in the diabatic and adiabatic models for different σ_x, other parameters (a.u.): ω_1=1, ω_2=1, a=4, A=5.0, b=-11, Δ=12, α=0.1, c=2, and σ_y=0.849.

Figure 4. Modulus of the adiabatic wavefunctions (|Φ|) in the one-state adiabatic models with (a) and without (b) GP for parameters (a.u.): ω_1=1, ω_2=1, a=4, A=5.0, b=-11, Δ=12, α=0.1, c=2, σ_x=1.274, and σ_y=0.849. The position of the CI is marked as a red dot. (c) Relative phase between the clockwise and counter-clockwise wave packets (t=5000 a.u. as an example) at x=3.1 a.u.

Fig. 1

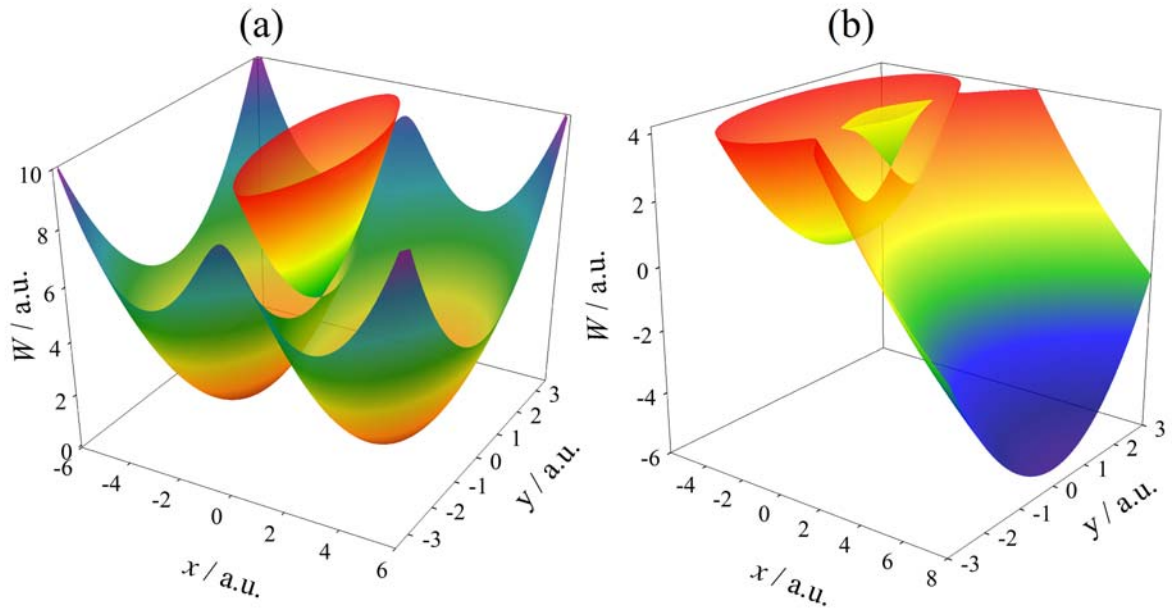

Fig. 2

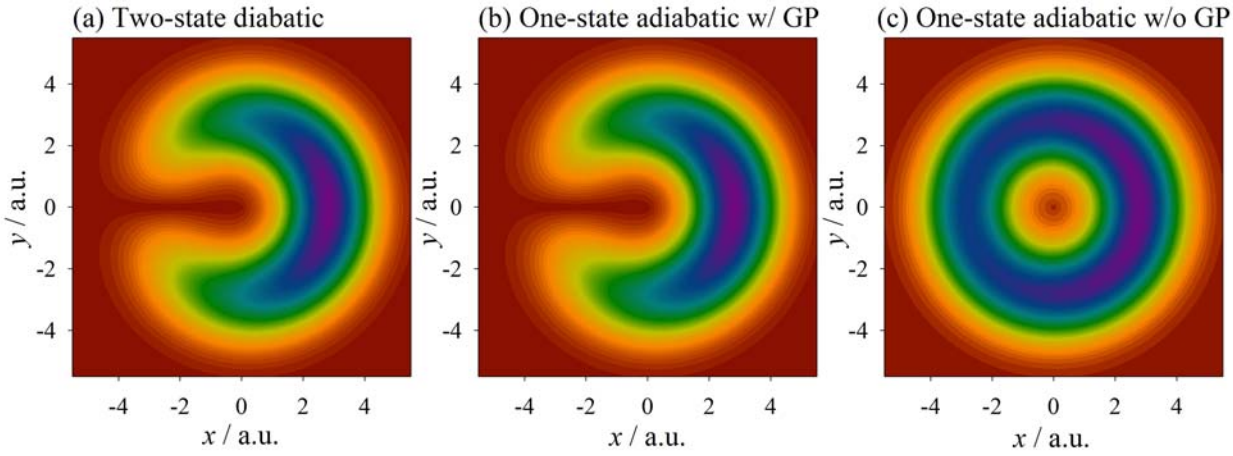
(a) Two-state diabatic
(b) One-state adiabatic w/ GP
(c) One-state adiabatic w/o GP
y / a.u.
x / a.u.
4
2
0
-2
-4

Fig. 3

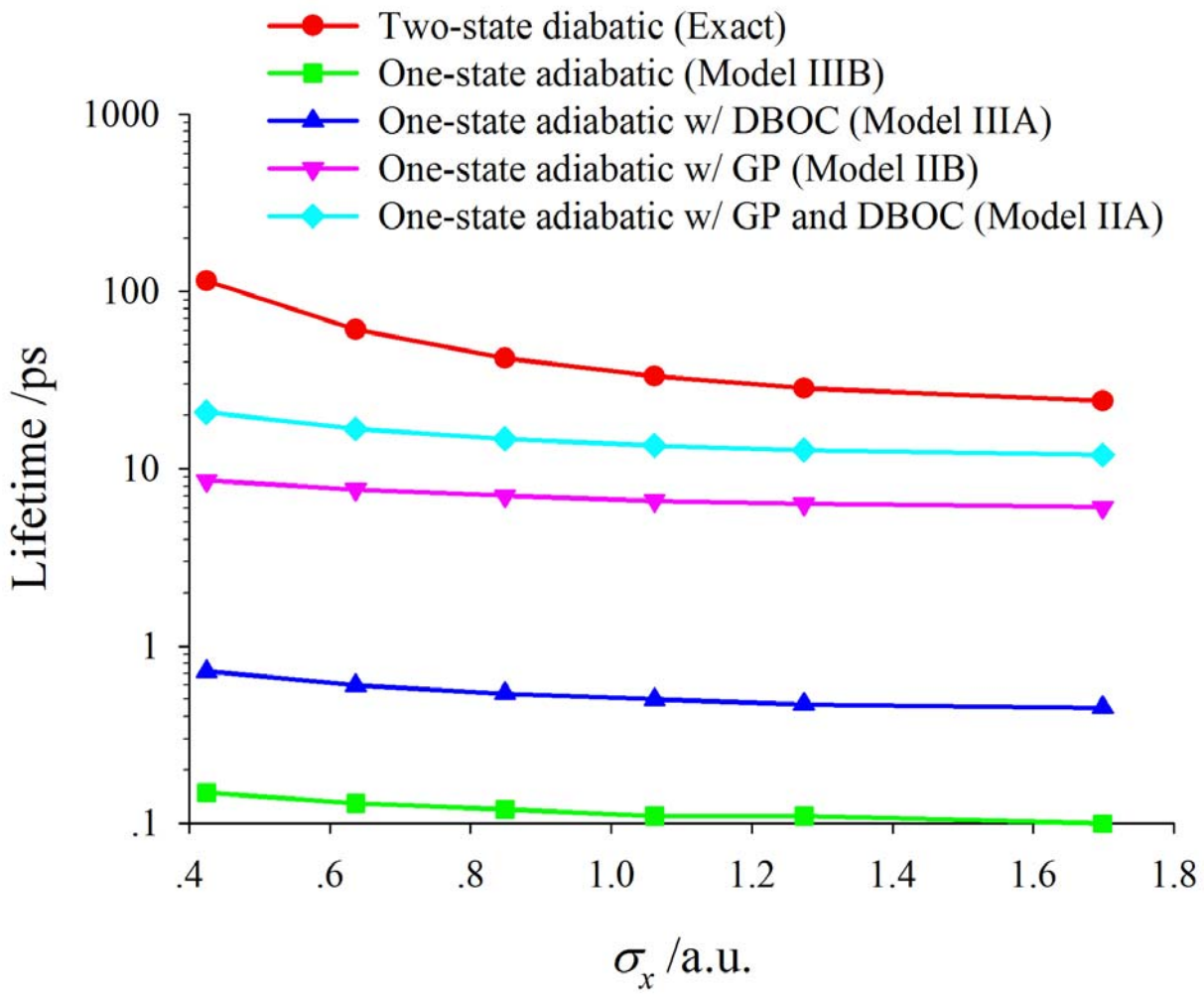
Two-state diabatic (Exact)
One-state adiabatic (Model IIIB)
One-state adiabatic w/ DBOC (Model IIIA)
One-state adiabatic w/ GP (Model IIB)
One-state adiabatic w/ GP and DBOC (Model IIA)
Lifetime /ps
1000
100
10
1
.1
.4
.6
.8
1.0
1.2
1.4
1.6
1.8
σ_x /a.u.

Fig. 4

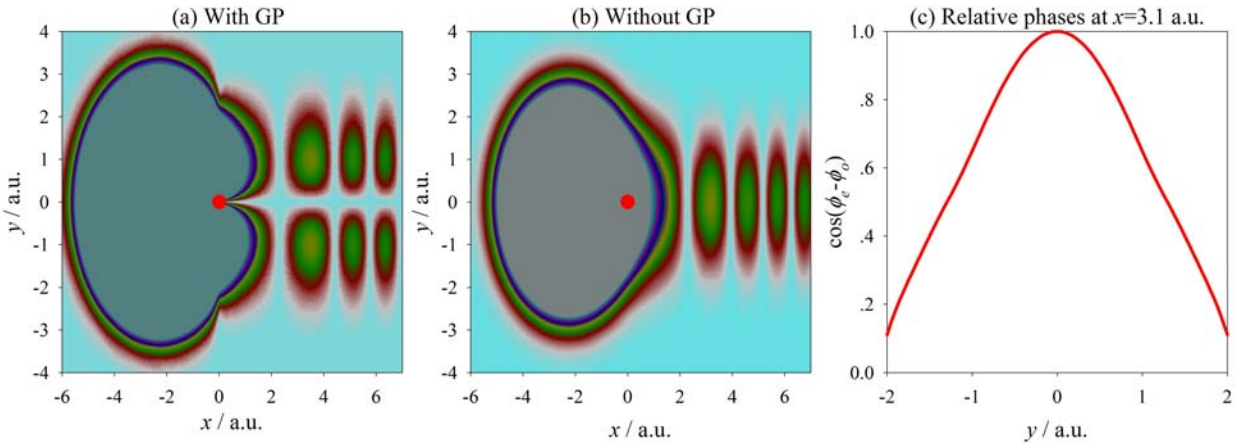
(a) With GP
(b) Without GP
(c) Relative phases at x=3.1 a.u.
y / a.u.
x / a.u.
$\cos(\phi_e - \phi_o)$
y / a.u.